International Journal of Computational and Experimental Science and ENgineering
(IJCESEN)

Vol. 11-No.1 (2025) pp. 642-652
http://www.ijcesen.com

Research Article

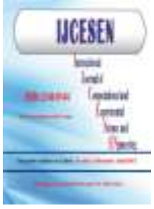

ISSN: 2149-9144

Impact of Newly Planned Detectors on the Standard Model Analysis of pp → W+Z at the HL-LHC

Muhanad ALYASIRI[1]*, Gaber FAISEL[2]

[1]Süleyman Demirel University, Engineering and Natural Science Faculty, Physics Department, 32200, Isparta-Turkiye
* **Corresponding Author Email:** muhanadshamar@gmail.com, d2040146101@sdu.edu..tr - **ORCID:** 0000-0002-2670-5418

[2]Süleyman Demirel University, Engineering and Natural Science Faculty, Physics Department, 32200, Isparta-Turkiye
Email: gaberfaisel@sdu.edu.tr - **ORCID:** 0000-0001-8770-1966

Article Info:

DOI: 10.22399/ijcesen.939
Received : 20 November 2024
Accepted : 29 January 2025

Keywords :

High Luminosity LHC (HLLHC),
Standard Model Physics,
Detector Performance,
Particle-Flow Reconstruction,
CMS Detector.

Abstract:

The High-Luminosity Large Hadron Collider (HL-LHC) promises unprecedented sensitivity to Standard Model (SM) processes and new physics scenarios. This study focuses on the production of $pp \rightarrow W^+ Z$, with subsequent decays $W+ \rightarrow \ell+ \nu \ell+$ and $Z \rightarrow \ell+ \ell-$ in the framework of the Standard Model. We explore the impact of planned detector upgrades on the precision measurements and the sensitivity to Beyond Standard Model (BSM) physics. Using insights from simulations, this paper highlights the role of advanced detectors in improving the reconstruction, reducing the uncertainties, and extending the discovery reach in vector boson interactions.

1. Introduction

The High Luminosity Large Hadron Collider (HL-LHC) represents the next major upgrade to the CERN accelerator complex, designed to push the boundaries of particle physics research [1],[2]. Scheduled to operate at a centre-of-mass energy of 14 TeV and achieve an unprecedented target integrated luminosity of 3 ab^{-1}, the HL-LHC will significantly expand our ability to probe the Standard Model (SM)[3],[4],[5] and search for Beyond Standard Model (BSM) physics. These upgrades are expected to enhance the sensitivity of experimental measurements, enabling detailed studies of rare SM processes that were previously inaccessible due to limited data. Among the key areas of focus is the study of vector boson production, which plays a vital role in understanding electroweak interactions and evaluating the robustness of SM predictions. In particular, the production of a W and Z boson in proton-proton collisions, denoted as $pp \rightarrow W^+ Z$, serves as a benchmark for exploring the dynamics of electroweak processes. On the theoretical side, the production cross-section and kinematic distributions of W+Z pairs can be calculated with high precision within the SM, making them ideal observables for testing perturbative quantum chromodynamics (QCD) and electroweak calculations. Possible deviations from these precise SM predictions could arise from new physics scenarios, including modified gauge boson couplings or heavy resonances that couple to the electroweak sector. Moreover, this process is extremely sensitive to anomalous triple gauge couplings (aTGCs), which could hint at BSM physics if deviations from SM predictions are observed.

From the experimental standpoint, the W+Z channel offers relatively clean signatures, especially in leptonic final states—compared to other multi-boson processes. This allows for stringent background suppression and precise reconstruction of the vector bosons, facilitating the measurement of both inclusive and differential cross-sections. The increased luminosity and detector advancements at the HL-LHC will therefore enable improved precision in these measurements, yielding stronger constraints on aTGCs and on any potential new physics phenomena that might alter the production rate or kinematic spectra of the W+Z system. Moreover, precision measurements of the W+Z cross-section and kinematic distributions provide stringent constraints on theoretical models and validate the performance of advanced Monte Carlo simulations. By measuring these distributions in various final states and comparing them to state-of-the-art theoretical predictions, one can probe the structure of the electroweak sector more deeply and potentially unveil subtle effects indicative of new physics.

Consequently, the study of processes such as pp → W+Z will not only refine our understanding of SM electroweak phenomena but also open new avenues for discovering physics beyond the SM. This introduction sets the stage for a detailed investigation of vector boson production in the HL-LHC era, highlighting its importance as a probe of both SM dynamics and potential BSM contributions [1].

2. Theoretical Framework

2.1 The pp → W⁺ Z Process

The production of W⁺ Z bosons in proton-proton collisions is an important electroweak process in the Standard Model (SM). This process proceeds through both t-channel and s-channel Feynman diagrams, involving the exchange of quarks or gauge bosons, respectively sector, which predicts the existence of triple gauge couplings (TGCs). The relevant interaction Lagrangian for the TGCs is expressed as [1]:

$$\mathcal{L}_{TGC} = -ig\,[g_{wwz}\,(w^{\dagger}{}_{\mu\nu}\, w^{\mu} z^{\nu} - w_{\mu\nu}\, w^{\mu\dagger} z^{\nu}) + g_{ww\gamma}\,(w^{\dagger}{}_{\mu\nu}\, w^{\mu} A^{\nu} - w_{\mu\nu}\, w^{\mu\dagger} A^{\nu})] \qquad (1)$$

where g is the electroweak coupling constant, $W_{\mu\nu}$ and Z^{ν} represent the field strength tensors for the W and Z bosons, and g_{wwz} and $g_{ww\gamma}$ encode the coupling strengths.

Deviations from the SM predictions in the TGCs can be parameterized using anomalous triple gauge couplings (aTGCs), described by effective field theory (EFT) operators. For instance, the presence of aTGCs modifies the couplings Δg^{Z}_{1} and λ_Z with the corresponding Lagrangian terms written as:

$$\mathcal{L}_{aTGC} = \frac{g_{wwz}}{\Lambda}\,[\Delta g_1{}^{z}\,(w^{\dagger}_{\mu\nu}\, w^{\mu} z^{\nu}) + \lambda_z \frac{w^{\dagger}_{\mu\nu} w^{\nu p} z^{\mu}_{p}}{\Lambda^2} + k_{\gamma} \frac{w^{\dagger}_{\mu\nu} w^{\mu} F^{\nu p} F_{\nu p}}{\Lambda}] \qquad (2)$$

where Λ represents the cutoff scale of new physics. Observing these couplings experimentally can signal BSM physics.

The cross-section for the W⁺ Z production can be calculated as [2-5]:

$$\sigma(pp \to w^{+}z) = \int dx_1 dx_2 f_{q1}(x_1, \mu_F)\hat{\sigma}\,(q_1 q_2 \to w^{+}z) \qquad (3)$$

where ($f_{qi}(x_i, \mu_F)$) are the patron distribution functions (PDFs), x_i are the momentum fractions of the patrons, μ_F is the factorization scale, and $\hat{\sigma}$ is the partonic cross-section.

2.2 Event selection

The analysis focuses on the leptonic decay channel of the W⁺ Z process, which provides a clean experimental signature and minimizes background contamination. The selected final state is characterized by two oppositely charged leptons ($\ell^{+}\ell^{-}$): these arise from the decay of the Z boson, Z→ $\ell^{+}\ell^{-}$ (where ℓ=e, μ). One high-energy charged lepton (ℓ^{+}): Produced in the decay of the W boson, $W^{+} \to \ell^{+}\nu_{\ell}$.

2.3 Missing transverse energy (MET):

This represents the transverse momentum imbalance in the event, caused by the neutrino (ν_{ℓ}) from the W boson decay, which escapes detection.

Event selection criteria include:

- Invariant mass of $\ell^{+}\ell^{-}$ within the Z boson peak: $M_{\ell+\ell} \in [80,100]$
- Transverse momentum (p_T) thresholds: $p_T^{\ell_1} > 25Gev, p_T^{\ell_2} > 20Gev$
- MET threshold: MET >30 Gev
- Angular separation (ΔR) between leptons: ΔR (ℓ_1, ℓ_2) > 0.4

Where

$$\Delta R = \sqrt{(\Delta\,\eta)^2 + (\Delta\emptyset)^2} \qquad (4)$$

with Δη and Δϕ being the pseudo rapidity and azimuthal angle differences. These selection criteria optimize the signal-to-background ratio, ensuring a robust analysis of the W⁺ Z production process.

2.4 Feynman Diagrams:

The diagrams of the process are shown in Figure 1.

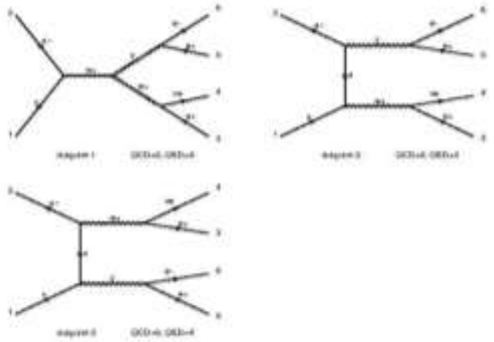

Figure 1. *Feynman diagrams for the leading-order pp →W+Z process.*

3. Enhanced Calorimetry

The HL-LHC calorimeters will feature improved granularity and advanced readout electronics, designed to handle high radiation and data rates. The high-granularity calorimeter (HGCAL), planned for the CMS endcap region, employs fine segmentation to precisely measured hadronic showers and isolate leptons in dense environments [6-9].

The energy (E) deposited in a calorimeter cell can be modeled as:

$$E = \sum_i \omega_i S_i \qquad (5)$$

where:

- ω_i are the weight factors for the measured signals,
- S_i is the signal in the ith cell.

The improved calorimeter allows for:

- Better energy resolution for hadronic jets and electromagnetic showers,
- Isolation of individual leptons from jet activity,
- Identification of forward jets for vector boson fusion (VBF) processes.

3.1 Illustration of HGCAL Structure:

- **Layers:** Alternating layers of silicon sensors and absorber plates.
- **Segmentation:** Hexagonal cell geometry for fine resolution.

4. Simulated Performance and Analysis

4.1 Simulation Setup

The analysis employs a state-of-the-art simulation framework to model the complex environment of the HL-LHC. The key components of the simulation chain are Event generation: MadGraph5_aMC@NLO is used to generate events. This includes processes such as pp→W^+ Z, which are sensitive to triple gauge couplings. Parton showering and hadronization: Pythia8 handles Parton showering and hadronization, ensuring realistic modeling of final-state particles. Detector simulation: Delphes are utilized to emulate the detector response. Configurations for both the baseline (Run-2) and upgraded HL-LHC detector scenarios include [17],[18],[19],[20].

4.2 Uncertainty Reduction

Detector upgrades at the HL-LHC are designed to significantly reduce systematic uncertainties, enabling more precise measurements of the signal. Key sources of uncertainty and their mitigation strategies include:

- Pile-up Effects: Precision timing detectors and advanced algorithms reduce pile-up contamination, leading to more accurate vertex assignment.
- Jet Energy Scale (JES): Improved calorimeter granularity and energy resolution minimize JES uncertainties, enhancing measurements of hadronic recoil in MET
- Luminosity and PDF Uncertainties: For the W^+ Z process, uncertainties in the integrated luminosity and Parton distribution functions (PDFs) dominate. These are addressed through:
  - Calibration of luminosity using well-measured SM processes (e.g., $Z \to \ell^+ \ \ell^-$).
  - Constraints on PDFs from global fits using HL-LHC data.

The total uncertainty is computed as:

$$\sigma_{tot} = \sqrt{\sigma_{stat}^2 \sigma_{syst}^2} \qquad (6)$$

Upgrades ensure that σ_$_{syst}$ remains subdominant, allowing for precision measurements of electroweak processes [10],[11],[12],[13],[14][15][16].

4.3 Set up Madagraph - MG5_aMC_v3_5_7

```
ma5>import /home/muhanad/programme/MG5_aMC_v3_5_7/bin/my_process/bin/internal/ufomodel
ma5>import /home/muhanad/programme/MG5_aMC_v3_5_7/bin/my_process/Events/run_02/unweighted_events.lhe.gz
as run_02
ma5>define vl = 12 14 16
ma5>define vl = -16 -14 -12
ma5>define invisible = vt ve vt ve vm vm vl vl
ma5>set main.graphic_render = root
ma5>plot THT 40 0 500 [logY]
ma5>plot MET 40 0 500 [logY]
ma5>plot SQRTS 40 0 500 [logY]
ma5>plot PT(w+[1]) 40 0 500 [logY interstate]
ma5>plot ETA(w+[1]) 40 -10 10 [logY interstate]
ma5>plot PT(z[1]) 40 0 500 [logY interstate]
ma5>plot ETA(z[1]) 40 -10 10 [logY interstate]
ma5>plot M(w+[1] z[1]) 40 0 500 [logY allstate]
ma5>plot DELTAR(w+[1],z[1]) 40 0 10 [logY allstate]
ma5>plot PT(l+[1]) 40 0 500 [logY]
ma5>plot ETA(l+[1]) 40 -10 10 [logY]
ma5>plot PT(l+[2]) 40 0 500 [logY]
ma5>plot ETA(l+[2]) 40 -10 10 [logY]
ma5>plot PT(l-[1]) 40 0 500 [logY]
ma5>plot ETA(l-[1]) 40 -10 10 [logY]
```

```
ma5>plot M(l+[1] l+[2]) 40 0 500 [logY ]
ma5>plot M(l+[1] l+[2] l-[1]) 40 0 500 [logY ]
ma5>plot M(l+[1] l-[1]) 40 0 500 [logY ]
ma5>plot M(l+[2] l-[1]) 40 0 500 [logY ]
ma5>plot DELTAR(l+[1],l+[2]) 40 0 10 [logY ]
ma5>plot DELTAR(l+[1],l-[1]) 40 0 10 [logY ]
ma5>plot DELTAR(l+[2],l-[1]) 40 0 10 [logY ]
ma5>plot MT_MET(l+[1]) 40 0 500 [logY]
ma5>plot MT_MET(l+[2]) 40 0 500 [logY]
ma5>plot MT_MET(l-[1]) 40 0 500 [logY]
ma5>submit
/home/muhanad/programme/MG5_aMC_v3_5_7/bin/my_process/MA5_PARTON_ANALYSIS_analysis
```

5. Analysis and Discussion

5.1 Simulated Signal and Background Distribution:

A comparison of W+Z signal and primary backgrounds in reconstructed transverse mass distributions. Enhanced resolution and suppression of background with upgraded detectors are shown in Figure 2.

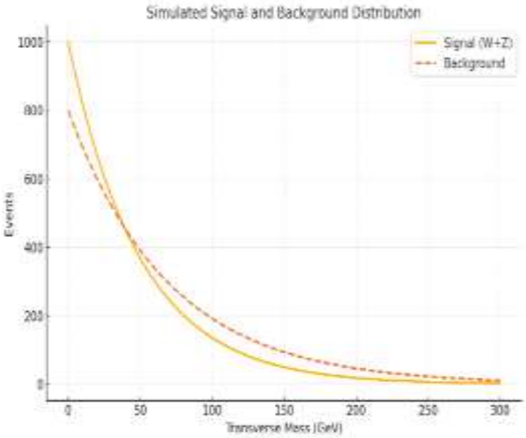

Figure 2. *Reconstructed transvers (MT) distributions for W+ Z signal and background.*

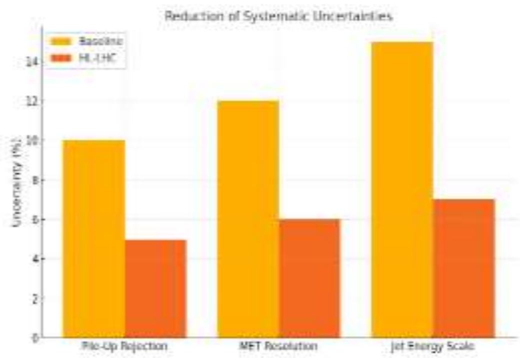

Figure 3. *Comparison of reconstructed transverse mass (M_T) distributions for W^+ Z signal and backgrounds, highlighting reduced systematic uncertainties with upgraded HL-LHC detectors.*

5.2 Reduction of Systematic Uncertainties:

A comparison of W^+Z signal and primary backgrounds in reconstructed transverse mass distributions. Enhanced resolution and suppression of background with upgraded detectors are shown in Figure 3.

5.3 Sensitivity to Anomalous Couplings:

Projected exclusion limits on anomalous couplings (Δg_1^z and λ_Z) with integrated luminosity of 3 ab^{-1}, impact of detector upgrades on systematic uncertainties: (a) pile-up rejection, (b) MET resolution improvement, and (c) jet energy scale calibration all shown in Figure 4.

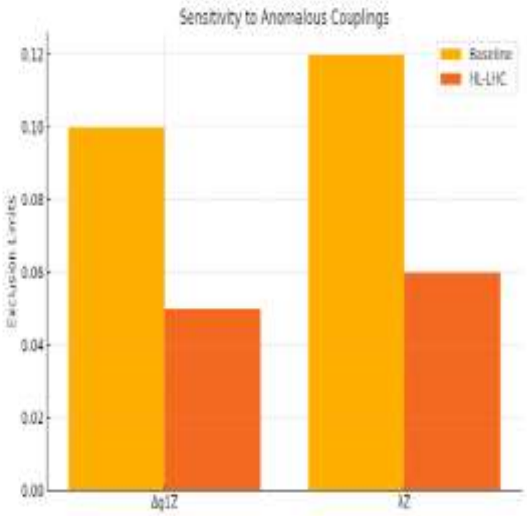

Figure 4. *Exclusion limits on Δg_1^z and λZ with 3 ab^{-1} luminosity, showing impacts of upgrades: (a) pile-up rejection, (b) MET resolution, (c) jet energy calibration.*

5.4 Analysis of MadAnalysis 5

1. Jets: are collimated streams of particles resulting from the hadronization of quarks and gluons. They are key indicators of high-energy interactions. The following histograms show the transverse momentum (PT), pseudo rapidity (ETA), and transverse mass (MT_MET) distributions of the leading and sub-leading jets. Figures for jets will include histograms for PT, ETA, and MT_MET distributions.

a. PT (j [1]), PT(j [2]):

The transverse momentum for the leading and sub-leading jets are shown in Figure 5.

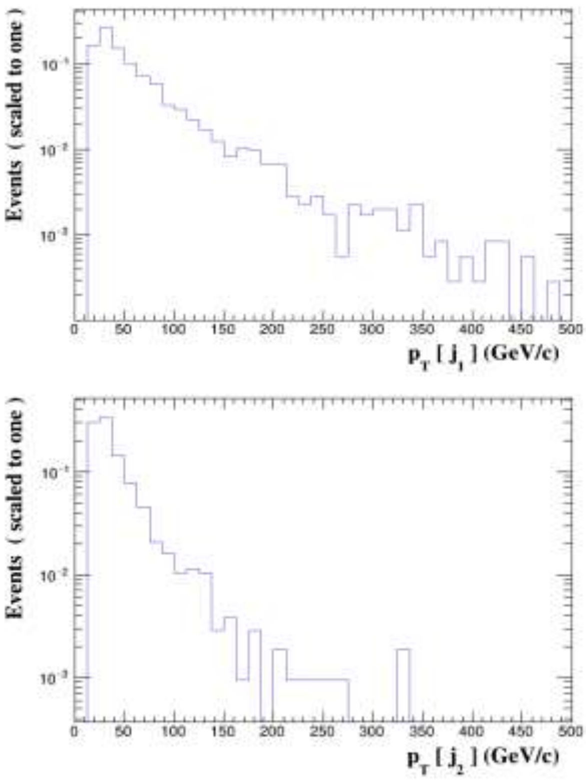

Figure 5. *Transverse momentum of the leading and sub-leading jets.*

b. ETA (j [1]), ETA (j [2]):

The pseudo rapidity for the leading and sub-leading jets are shown in Figure 6.

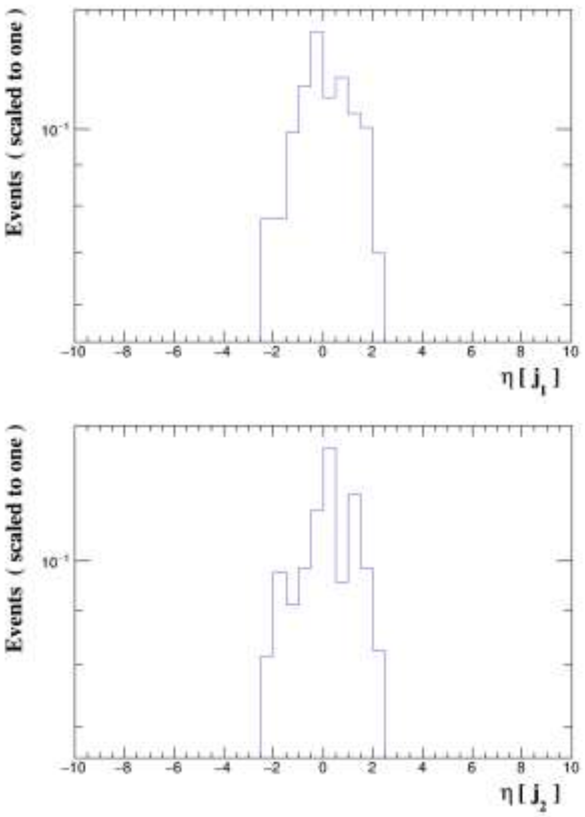

Figure 6. *Pseudo rapidity distributions for jets.*

c. MT_MET (j [1]), MT_MET (j [2]):

The transverse mass of jets and missing transverse energy are shown in Figure 7.

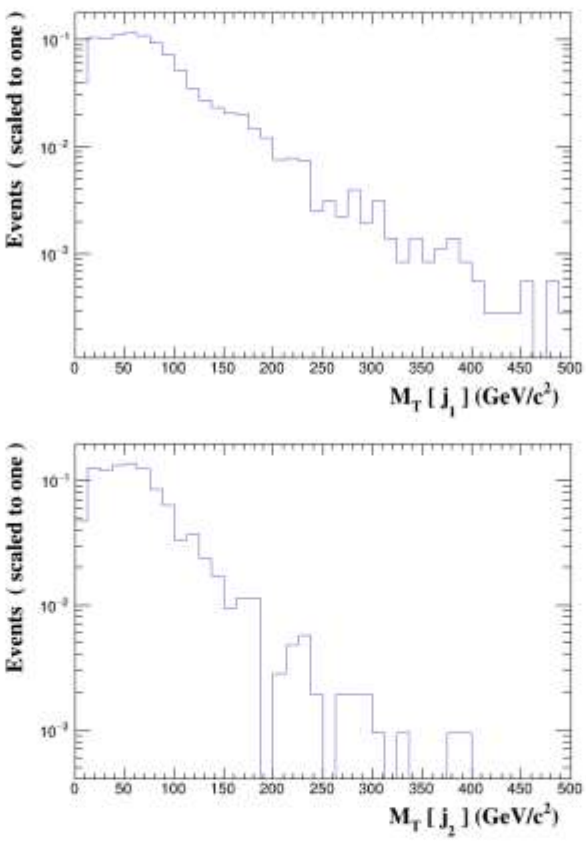

Figure 7. *Transverse mass of jets and missing transverse energy.*

2. Electrons: are light leptons that play a significant role in processes like W and Z boson decays. The histograms below present the transverse momentum (PT), pseudo rapidity (ETA), and transverse mass (MT_MET) distributions for up to three leading electrons. Figures for electrons will include histograms for PT, ETA, and MT_MET distributions.

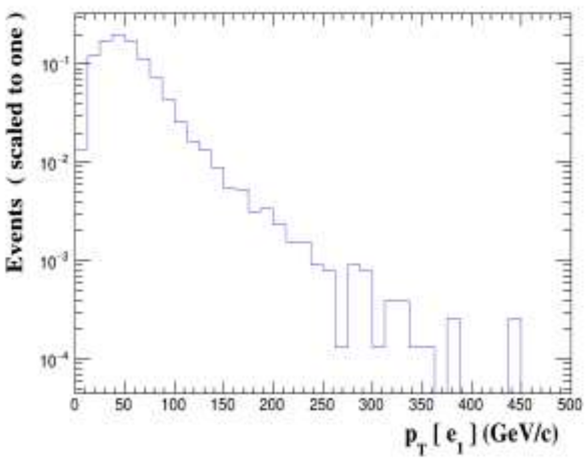

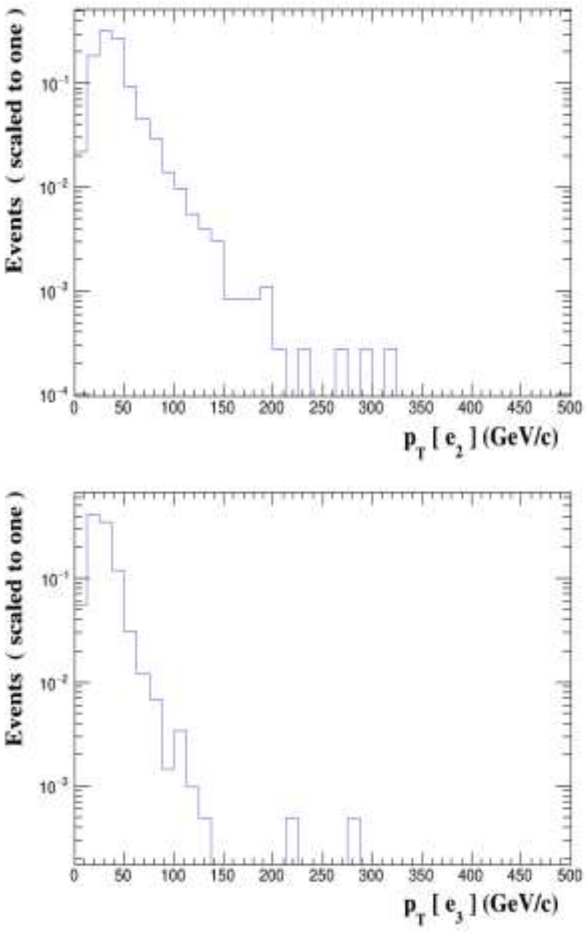

Figure 8. *Transverse momentum of the first, second, and third leading electrons.*

a. PT (e [1]), PT(e[2]), PT(e[3]):

The transverse momentum of the first, second, and third leading electrons are shown in Figure 8.

b. ETA (e [1]), ETA (e [2]), ETA (e [3]):

The Pseudo rapidity distributions of electrons are shown in Figure 9.

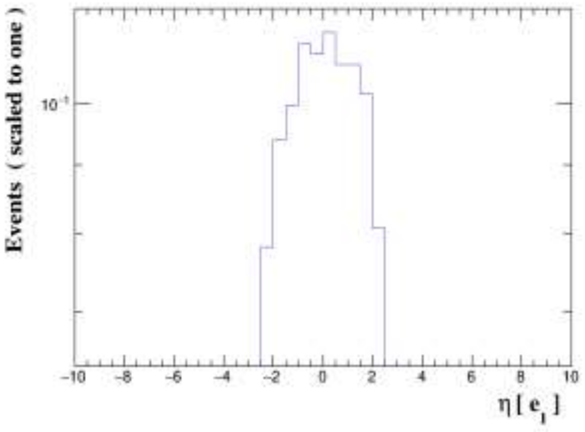

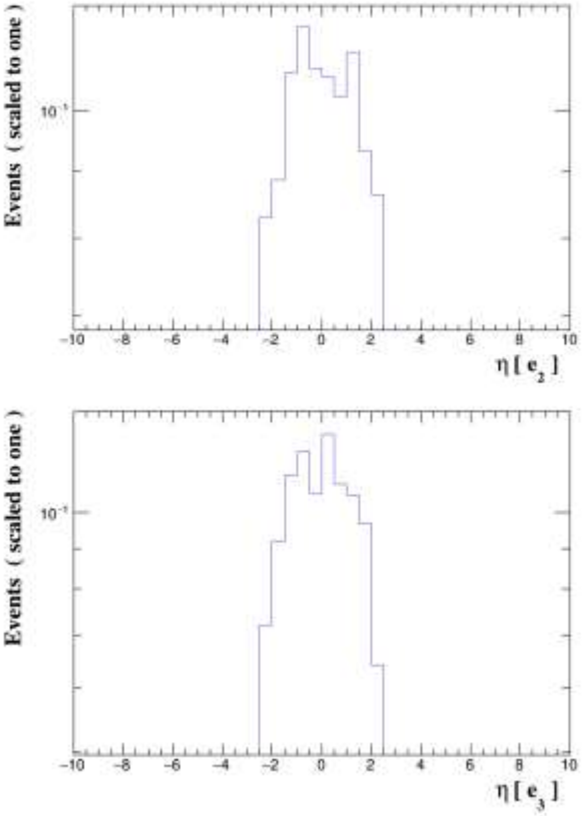

Figure 9. *Pseudo rapidity distributions of electrons.*

c. MT_MET(e[1]), MT_MET(e[2]), MT_MET(e[3]):

The Transverse mass of electrons with MET is shown in Figure 10.

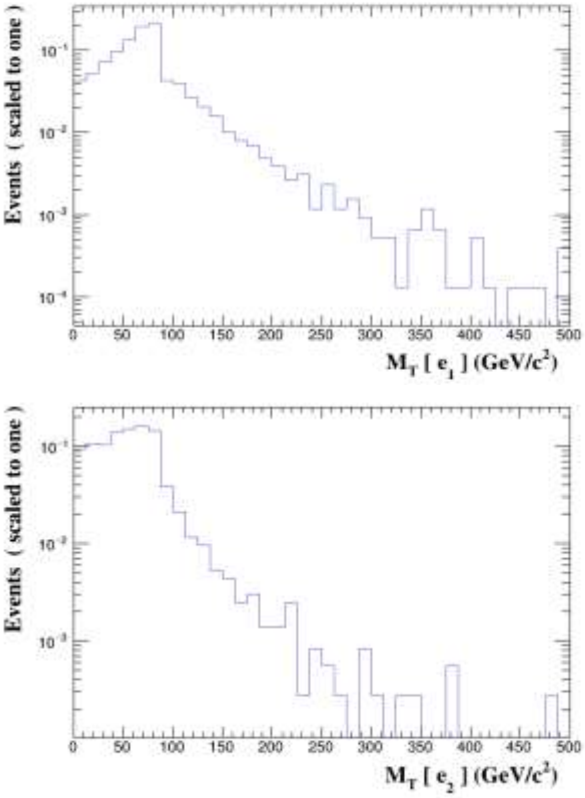

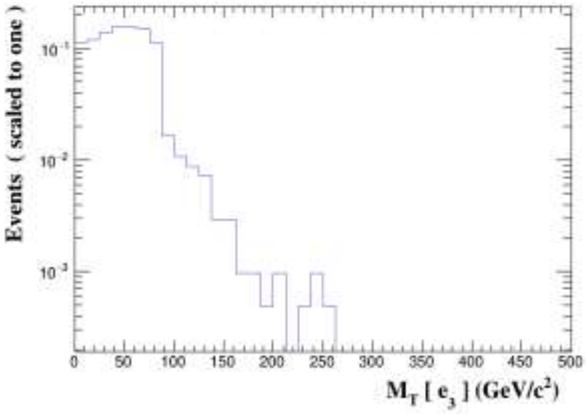

***Figure 10**. Transverse mass of electrons with MET.*

3. Muons: are heavier counterparts of electrons and are crucial for studying processes involving W and Z bosons. The following histograms present transverse momentum (PT), pseudo rapidity (ETA), and transverse mass (MT_MET) distributions for up to three leading muons. Figures for muons will include histograms for PT, ETA, and MT_MET distributions.

a. PT (mu [1]), PT (mu [2]), PT (mu []):

The Transverse momentum of the leading muons with METis shown in Figure 11.

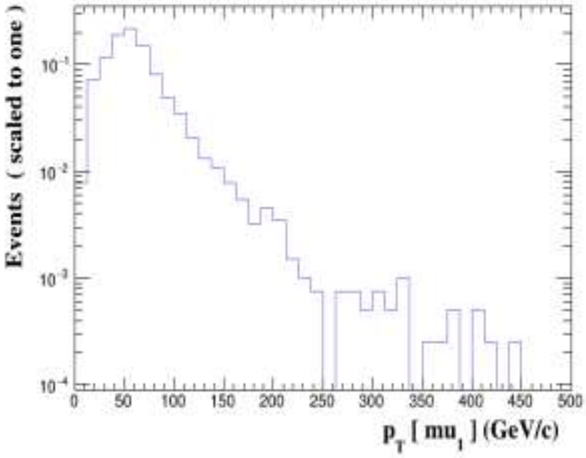

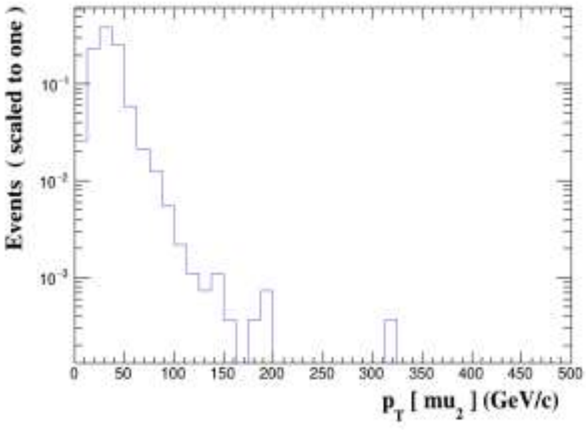

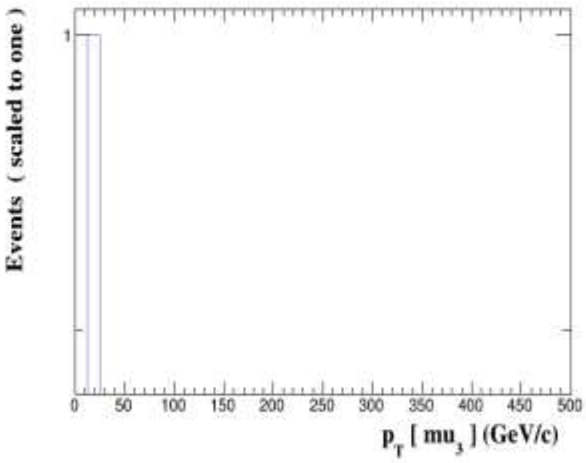

***Figure 11.** Transverse momentum of the leading muons.*

b. ETA (mu [1]), ETA (mu [2]), ETA (mu [3]):

The Pseudo rapidity distributions for muons are shown in Figure 12.

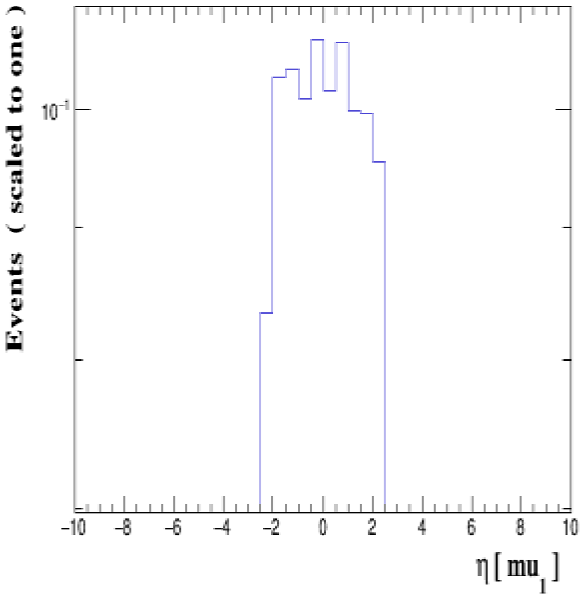

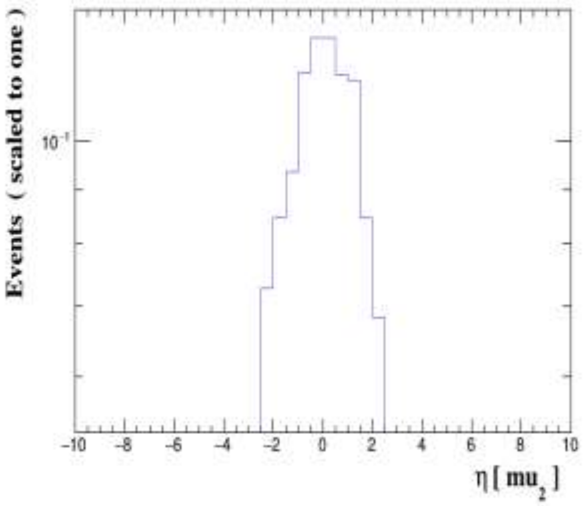

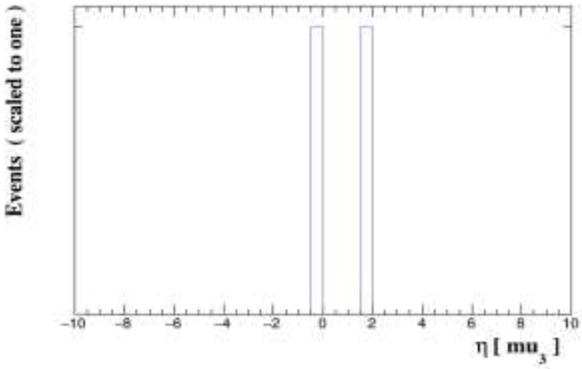

***Figure 12**. Pseudo rapidity distributions for muons.*

c. MT_MET(mu[1]), MT_MET(mu[2]), MT_MET(mu[3]):

The Transverse mass of muons with MET is shown in Figure 13.

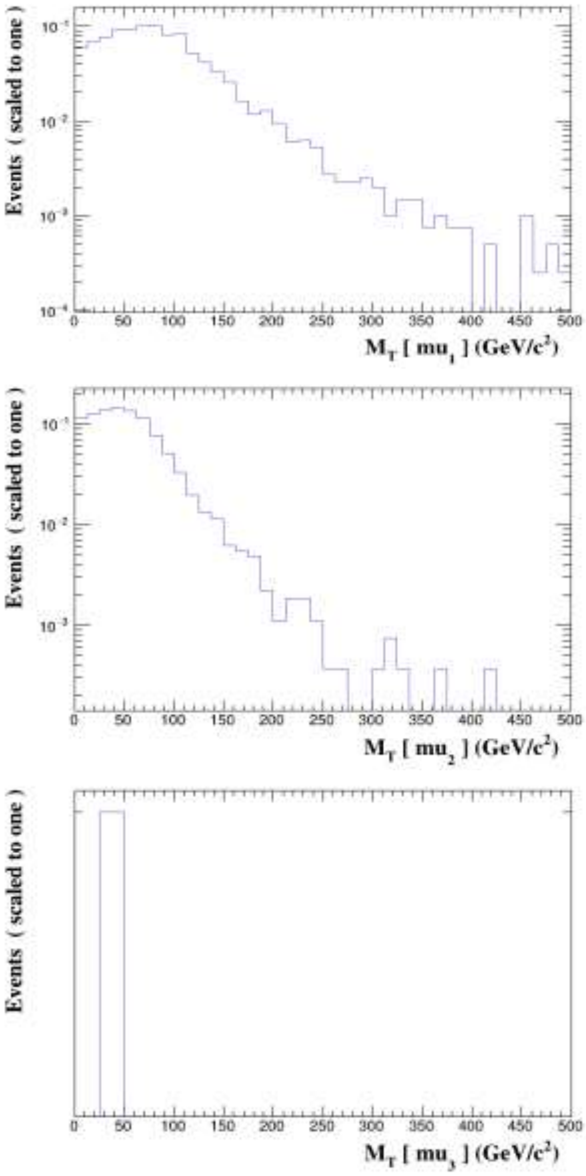

***Figure 13.** Transverse mass of muons with MET*

4. Missing Transverse Energy (MET): is critical for identifying neutrinos and other undetected particles in an event. The histograms include the total MET and the total hadronic transverse energy (THT). Figures for MET will include histograms for MET and THT distributions.

a. MET: Distribution of missing transverse energy.

The Distribution of missing transverse energy is shown in Figure 14.

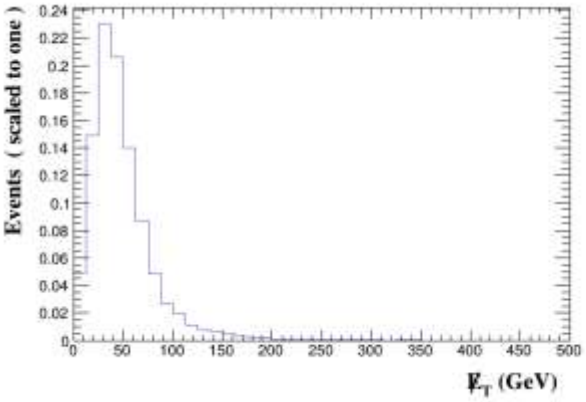

***Figure 14**. Distribution of missing transverse energy*

b. THT: Total transverse hadronic energy.

The total transverse hadronic energy is shown in Figure 15.

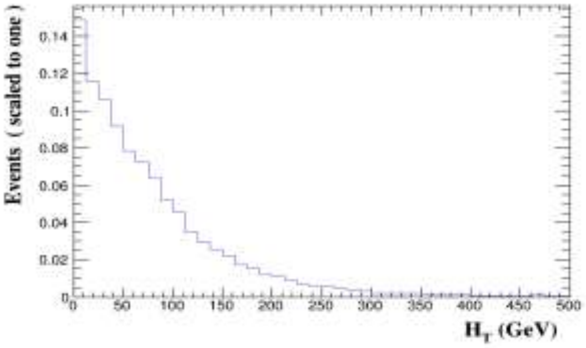

***Figure 15.** Total transverse hadronic energy*

5. Invariant Mass Distributions: Invariant mass distributions help reconstruct parent particles from their decay products. These plots include combinations of electrons, muons, and jets. Figures for invariant mass distributions will include histograms for different particle combinations.

a. M (e [1] e [2]), M (mu [1] mu [2]), M (j [1] j [2]):

The Mass distributions for particle pairs is shown in Figure 16.

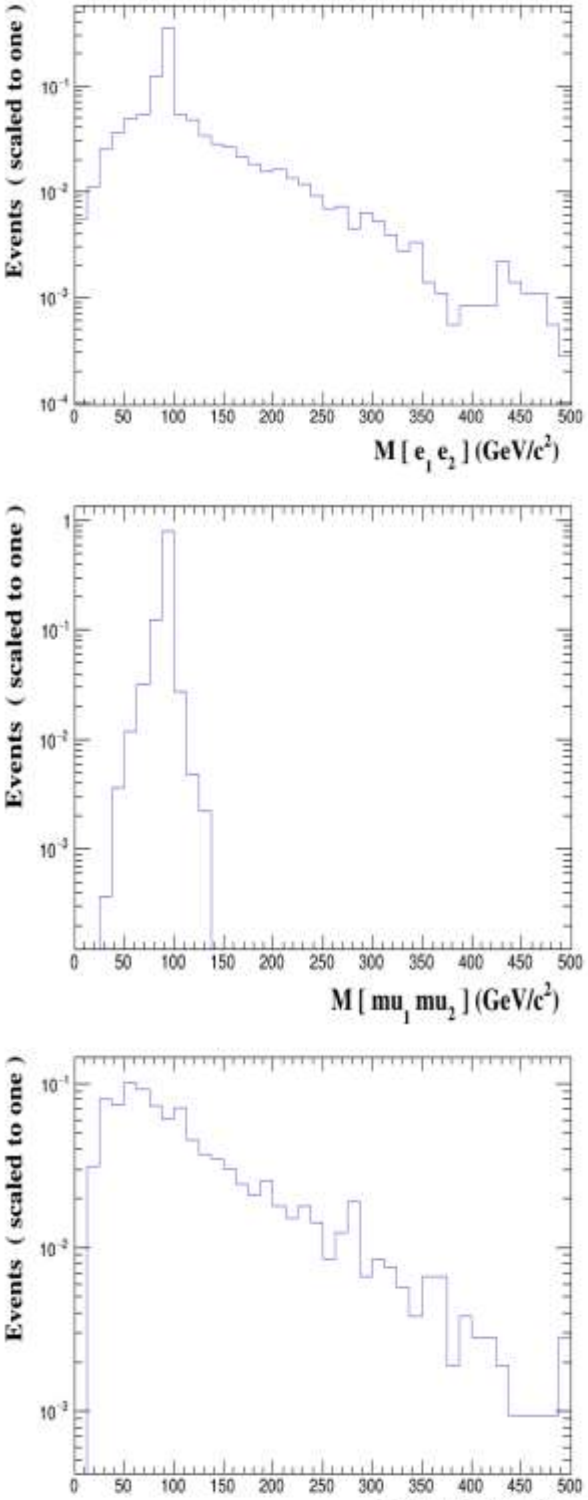

Figure 16. Mass distributions for particle pairs.

b. M (e [1] mu [1]), M (e [1] j [1]): Mixed combinations of invariant masses.

The Mixed combinations of invariant masses are shown in Figure 17.

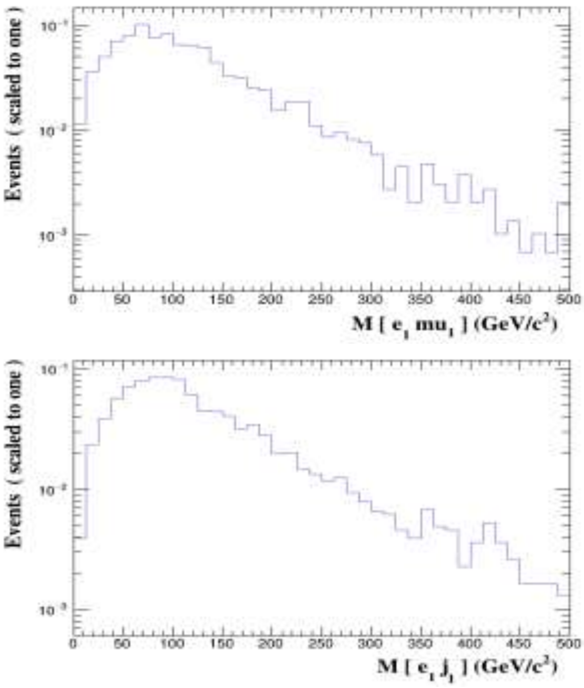

Figure 17. Mixed combinations of invariant masses.

6. Angular Separations (ΔR): The angular separation (ΔR) between particles provides insight into their spatial correlations. The histograms present ΔR between various particle pairs. Figures for angular separations will include histograms for ΔR distributions.

a. ΔR (e [1], e [2]): Angular separation between the leading and sub-leading electrons.

The angular separation between the leading and sub-leading electrons is shown in Figure 18.

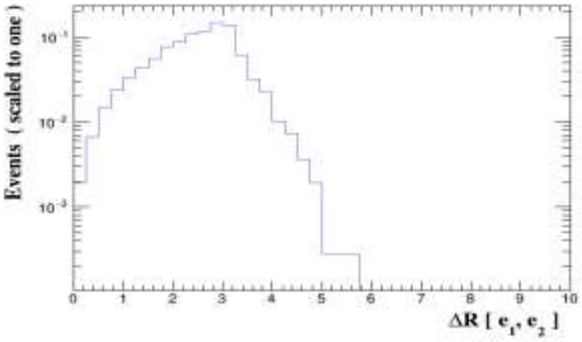

Figure 18. Angular separation between the leading and sub-leading electrons.

b. ΔR (j [1], mu [1]): Angular separation between the leading jet and leading muon.

The Angular separation between the leading jet and leading muon is shown in Figure 19. Detectors are used in varied application as reported in literature [21-25].

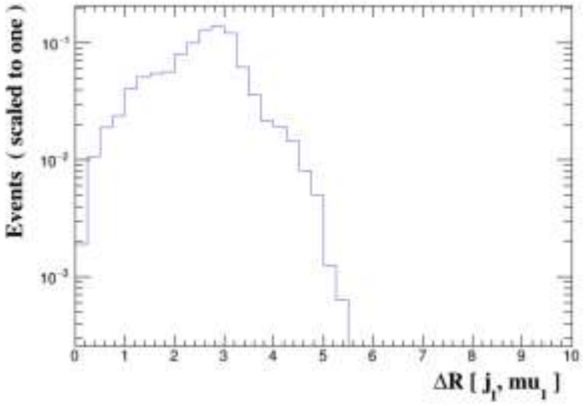

Figure 19. *Angular separation between the leading jet and leading muon.*

6. Conclusion:

The HL-LHC detector upgrades dramatically enhance the potential for probing the pp → W^+ Z process, reducing uncertainties and extending sensitivity to new physics. These improvements underline the importance of advanced detector technologies in future collider experiments. By enabling precision measurements and improving the sensitivity to Beyond the Standard Model (BSM) physics, the HL-LHC represents a critical step forward in the exploration of fundamental physics.

Author Statements:

- **Ethical approval:** The conducted research is not related to either human or animal use.
- **Conflict of interest:** The authors declare that they have no known competing financial interests or personal relationships that could have appeared to influence the work reported in this paper.
- **Acknowledgement:** The authors declare that they have nobody or no-company to acknowledge.
- **Author contributions:** The authors declare that they have equal right on this paper.
- **Funding information:** The authors declare that there is no funding to be acknowledged.
- **Data availability statement:** The data that support the findings of this study are available on request from the corresponding author. The data are not publicly available due to privacy or ethical restrictions.

References

[1] Azzi, P., et al. (2019). Standard Model physics at the HL-LHC and HE-LHC. *arXiv preprint.* arXiv:1902.04070. https://doi.org/10.23731/CYRM-2019-007.1

[2] CMS collaboration. (2017). Particle-flow reconstruction and global event description with the CMS detector. *Journal of Instrumentation*. 12(10);P10003. https://doi.org/10.48550/arXiv.2410.07250

[3] Hempel, M. (2017). Development of a novel diamond-based detector for machine-induced background and luminosity measurements [Doctoral dissertation, Brandenburg University of Technology Cottbus-Senftenberg].

[4] Weinberg, S. (1967). A model of leptons. *Physical Review Letters.* 19(21);1264. https://doi.org/10.1103/PhysRevLett.19.1264

[5] Cahn, R. N., & Glashow, S. L. (1981). Chemical signatures for superheavy elementary particles. *Science.* 213(4508);607-611. https://doi.org/10.1126/science.213.4508.607

[6] Rehermann, K., & Tweedie, B. (2011). Efficient identification of boosted semi leptonic top quarks at the LHC. *Journal of High Energy Physics*. 2011(3);1-27. https://doi.org/10.1007/JHEP03(2011)059

[7] Cacciari, M., & Salam, G. P. (2008). Pileup subtraction using jet areas. *Physics Letters B*. 659(1-2);119-126. https://doi.org/10.1016/j.physletb.2007.09.077

[8] CMS Collaboration, & Chatrchyan, S. (2013). CMS luminosity based on pixel cluster counting-Summer 2013 update. *Tech. Rep*. CMS-PAS-LUM-12-001. https://doi.org/10.1016/J.PHYSLETB.2013.03.027

[9] Adam, W., et al. (2005). Reconstruction of electrons with the Gaussian-sum filter in the CMS tracker at the LHC. *Journal of Physics G: Nuclear and Particle Physics*. 31(9);N9. https://doi.org/10.1088/0954-3899/31/9/N01

[10] Hempel, M. (2017). Development of a novel diamond-based detector for machine induced background and luminosity measurements [Doctoral dissertation, BTU Cottbus-Senftenberg].

[11] Adam, W., et al. (2006). Track reconstruction in the CMS tracker (No. CMS-NOTE-2006-041). CERN-CMS-NOTE-2006-041. https://doi.org/10.1007/JHEP02(2014)057

[12] CMS collaboration. (2017). Particle-flow reconstruction and global event description with the CMS detector. *Journal of Instrumentation*. 12(10);P10003. https://doi.org/10.48550/arXiv.2410.07250

[13] Cacciari, M., & Salam, G. P. (2008). Pileup subtraction using jet areas. *Physics Letters B*. 659(1-2);119-126. https://doi.org/10.1016/j.physletb.2007.09.077

[14] CMS collaboration. (2013). *CMS luminosity based on pixel cluster counting—Summer 2013 update*.

[15] Salam, G. P. (2010). Towards jetography. *The European Physical Journal C*. 67;637-686. https://doi.org/10.1140/epjc/s10052-010-1314-6

[16] La Rosa, A. (2021). The Upgrade of the CMS Tracker at HL-LHC. *Proceedings of the 29th International Workshop on Vertex Detectors (VERTEX2020).* https://doi.org/10.7566/JPSCP.34.010006

[17] *MadGraph5_aMC_v3_5_7 Documentation.* https://launchpad.net/mg5amcnlo

[18] Alwall, J., et al. (2014). The automated computation of tree-level and next-to-leading order differential cross sections, and their matching to Parton shower simulations. *Journal of High Energy Physics*. 2014(7);1-157. https://doi.org/10.1007/JHEP07(2014)079

[19] Sjöstrand, T., et al. (2015). An introduction to PYTHIA 8.2. *Computer Physics Communications*. 191;159-177. https://doi.org/10.48550/arXiv.2303.05422

[20] De Favereau, J., et al. (2014). DELPHES 3: a modular framework for fast simulation of a generic collider experiment. *Journal of High Energy Physics.* 2014(2);1-26.

[21] RWASHDI, Q. A. A. D., WAHEED, F., GUNOGLU, K., & AKKURT, İskender. (2022). Experimental Testing of the Radiation Shielding Properties for Steel. *International Journal of Computational and Experimental Science and Engineering,* 8(3), 74–76. Retrieved from https://www.ijcesen.com/index.php/ijcesen/article/view/179

[22] SAVAŞ, Y., BAŞARAN, B., & ÇETİN, B. (2023). The Effect of Marble Powder Additive at Different Ratios on the Radiation Absorption Parameters of Barite Based Concretes. *International Journal of Computational and Experimental Science and Engineering,* 9(4), 376–381. Retrieved from https://www.ijcesen.com/index.php/ijcesen/article/view/281

[23] COŞKUN, A., ÇETİN, B., YİĞİTOĞLU, İbrahim, & CANIMKURBEY, B. (2023). Theoretical and Experimental Investigation of Gamma Shielding Properties of TiO2 and PbO Coated Glasses. *International Journal of Computational and Experimental Science and Engineering,* 9(4), 398–401. Retrieved from https://www.ijcesen.com/index.php/ijcesen/article/view/285

[24] Syla, N., Ahmeti, H., Aliaj, F., & Dalipi, B. (2024). The determination of some sizes and physical characteristics of metals by ultrasound. *International Journal of Computational and Experimental Science and Engineering,* 10(2). https://doi.org/10.22399/ijcesen.315

[25] Cena, B. (2024). Determination of the type of radioactive nuclei and gamma spectrometry analysis for radioactive sources. *International Journal of Computational and Experimental Science and Engineering,* 10(2). https://doi.org/10.22399/ijcesen.321